UC Irvine
UC Irvine Previously Published Works

Title

Analyses and design for electrochemical migration suppression by alloying indium into silver

Permalink
https://escholarship.org/uc/item/8nj9q4f3

Journal
Journal of Materials Science: Materials in Electronics, 29(16)

ISSN
0957-4522

Authors
Yang, CA
Wu, J
Lee, CC
et al.

Publication Date
2018-08-01

DOI
10.1007/s10854-018-9520-3

Peer reviewed

eScholarship.org Powered by the California Digital Library
University of California

Journal of Materials Science: Materials in Electronics (2018) 29:13878–13888
https://doi.org/10.1007/s10854-018-9520-3

Analyses and design for electrochemical migration suppression by alloying indium into silver

C. A. Yang[1,3] · J. Wu[3] · C. C. Lee[3] · C. R. Kao[1,2]

Received: 8 May 2018 / Accepted: 19 June 2018 / Published online: 22 June 2018
© Springer Science+Business Media, LLC, part of Springer Nature 2018

Abstract
Silver electrochemical migration (ECM) is a serious reliability issue for fine pitch as well as power electronic devices that employ silver as interconnection materials. In this study, a method to suppress the ECM behavior of silver was proposed and implemented. Solid solutions of Ag–In and intermetallic compounds were fabricated and their ECM properties were studied through the water drop test (WDT). The WDT was performed on alumina substrate in deionized water at 3 V, where the leakage current was measured. The results show that Ag–In alloy samples have considerably longer lifetime before reaching short circuit than pure silver samples. As indium concentration in Ag–In solid solution increases, the resistance to ECM also increases. The migration process is completely inhibited when the indium concentration reaches 19 at.%. The morphologies of the dendrites and surfaces of the anode and cathode were also investigated. A model was established to explain the anti-ECM mechanism of Ag–In alloys. By forming indium oxide on the surface of the anode under electric field in a humid environment, the anode gets passivated and the silver dissolution path is completely blocked, and thus inhibiting the ECM process. It was discovered that the quality of electrode surfaces is essential in realizing the full potential of the inherent anti-ECM ability of Ag–In alloys. In conclusion, the results of this investigation have shown that Ag–In alloys can be promising and valuable candidates for conductors, metallization, and interconnect materials in fine pitch and high power electronic devices.

1 Introduction

The increasing demand of high integration density and small packaging size has driven the development of fine pitch technology for electronic packaging. However, the miniaturization of electronic components has led to reliability issues such as electrochemical migration (ECM) failure. With the presence of moisture and an electric field, commonly used conductor metals such as Ag, Cu [1, 2], and Sn-based alloys [1, 3] are electrochemically unstable and tend to dissolute through anodic ionization. The solvated metal ions will migrate across the electrolytic solution along the electric field and re-deposit at the cathode [3]. Subsequently, a conducting filament, or dendrite, will grow out of the cathode and eventually bridge the cathode and anode, resulting in a short circuit in electronic devices. The situation will be even worse under high temperature conditions and high electric field [3–5], making the ECM reliability issue more critical in high power modules.

To improve the resistance of electronic components to ECM failure, various electrode and surface finish materials and relevant processing optimization techniques have been proposed, such as the Ag–Pd alloys [6, 7], Cu–Sn intermetallic compound barrier [2], and the directly printed Ag with optimized sintering condition [4], etc. In the studies of Ag–Pd alloys, Lin and Chan [6, 7] found that as the concentration of Pd in the alloy increases, the resistance to ECM increases, and the ECM process was completely inhibited when 30% of Pd was alloyed in Ag. They proposed that the inhibition mechanism came from the anodic surface passivation by PdO, which results from the higher oxidation potential of Pd than Ag in the alloy. However, the high cost of Pd is still a concern for industries to utilize Ag–Pd alloys widely.

Ag–In alloys have been proven to have superior mechanical properties, thermal cycling reliability, high temperature reliability and anti-tarnishing properties in our previous

✉ C. R. Kao
crkao@ntu.edu.tw

1 Department of Materials Science and Engineering, National Taiwan University, Taipei, Taiwan

2 Advanced Research Center of Green Materials Science and Technology, National Taiwan University, Taipei, Taiwan

3 Department of Electrical Engineering and Computer Science, University of California, Irvine, CA, USA

studies [8–12], which make them excellent packaging materials for die attachment as well as interconnection materials, especially in power electronics. Therefore, the study of the ECM property of the Ag–In alloys becomes essential and critical, which has not yet been reported in literature. In this study, the behaviors and susceptibilities of ECM of four specific Ag–In alloys and two pure silver materials were examined via the water drop test (WDT) in deionized water and applied electric field. The WDT is a commonly used accelerated testing method for the measurement of ECM resistance [1–7, 13–16]. The compositions of all the tested samples are: Ag, Ag–In solid solutions with 10 at.% In and 19 at.% In (which will be denoted as (Ag)-10In and (Ag)-19In in the following article), Ag_3In and Ag_9In_4, as labeled in the Ag–In binary phase diagram in Fig. 1 [17]. The effect of indium concentration on the ECM behavior was also investigated in this study.

2 Experimental procedure

2.1 Materials preparation

The electrode samples in this study were fabricated by two methods: casting and sintering. The casting method was chosen for the preparation of ductile materials in the form of ingots, including pure silver, (Ag)-10In, (Ag)-19In and Ag_3In. 4N silver and indium shots were weighed, uniformly mixed and loaded in quartz tubes. Then the quartz tubes were pumped by a vacuum pump and sealed by a hydrogen–oxygen torch to form a capsule. The vacuum environment during casting can reduce the oxidation reaction and the formation of voids or defects by trapped bubbles inside the ingots. Next, each capsule was placed into a furnace at 1020 °C for homogenization and then cooled down to room temperature following a four-stage cooling profile. After the homogenous ingots with four different compositions were produced, a rolling process was conducted to fabricate foils with the thickness of approximately 150 µm. Prior to the WDT, the foils were polished and cleaned, and the final thicknesses were measured to be 120 µm.

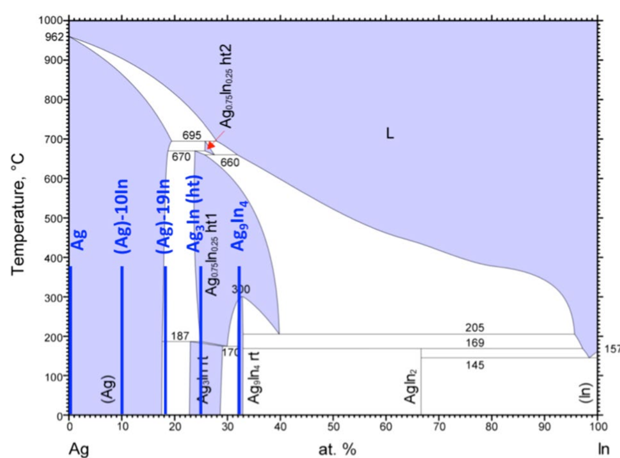

Fig. 1 Ag–In binary phase diagram showing the compositions of all the tested samples in this study [17]

On the other hand, sintering method with 100 µm nano-silver paste and 10 µm indium foil was utilized to fabricate the brittle Ag–In intermetallic compound, Ag_9In_4. Sintered nano-silver electrode was also fabricated with 100 µm nano-silver paste as a reference of pure silver for the sintered electrode samples. Nano-silver pastes in both samples were printed on the alumina substrate (96% Al_2O_3) with a pair of rectangular shape in the dimension of 15 mm (L) x 5 mm (W). Next, the pastes underwent a pre-curing step at 130 °C for 70 s in air, and a pressureless sintering process for 30 min from room temperature to peak temperature of 300 °C under 0.1 torr vacuum. The fabrication process for both sintered electrode samples is shown in Fig. 2a. The microstructure and elemental mappings of the sintered Ag_9In_4 electrode analyzed by scanning electron microscopy (SEM) and energy dispersive X-ray spectroscopy (EDX) were shown in Fig. 2b–e. The composition of the sintered Ag_9In_4 electrode was quite uniform. X-ray diffractometer (XRD) identifications were also carried out to verify the phases and compositions of the sample, which are shown in the following section. As for the porosity of the sintered nano-silver electrode and sintered Ag_9In_4 electrode in our study, it was around 30 and 15 vol%, respectively, which was measured by the cross-sectional SEM images based on the quantitative metallography method.

2.2 Phase identification and chemical composition examination

The fabricated foils and sintered electrodes were examined by XRD, SEM and EDX to confirm their phases as well as compositions. Rigaku SmartLab XRD was used in the Bragg–Brentano (BB) operation mode with a scanning speed of 2°/min. After XRD measurement, the collected data were analyzed by PDXL, an integrated powder X-ray analysis software package. The XRD patterns and crystallographic information of the electrode samples are shown in Fig. 3 and Table 1.

Each electrode sample contained only one phase, showing good uniformity of all the electrode samples. Besides, both of the diffraction patterns of (Ag)-10In and (Ag)-19In resemble the pattern of pure silver, all representing a face-centered cubic (FCC) crystal structure. However, their peaks shift a certain degree towards the left because of the increase in lattice constants as indium concentration increases. FEI/Philips XL-30 FEG SEM and EDX were used to measure the chemical compositions of the silver–indium solid

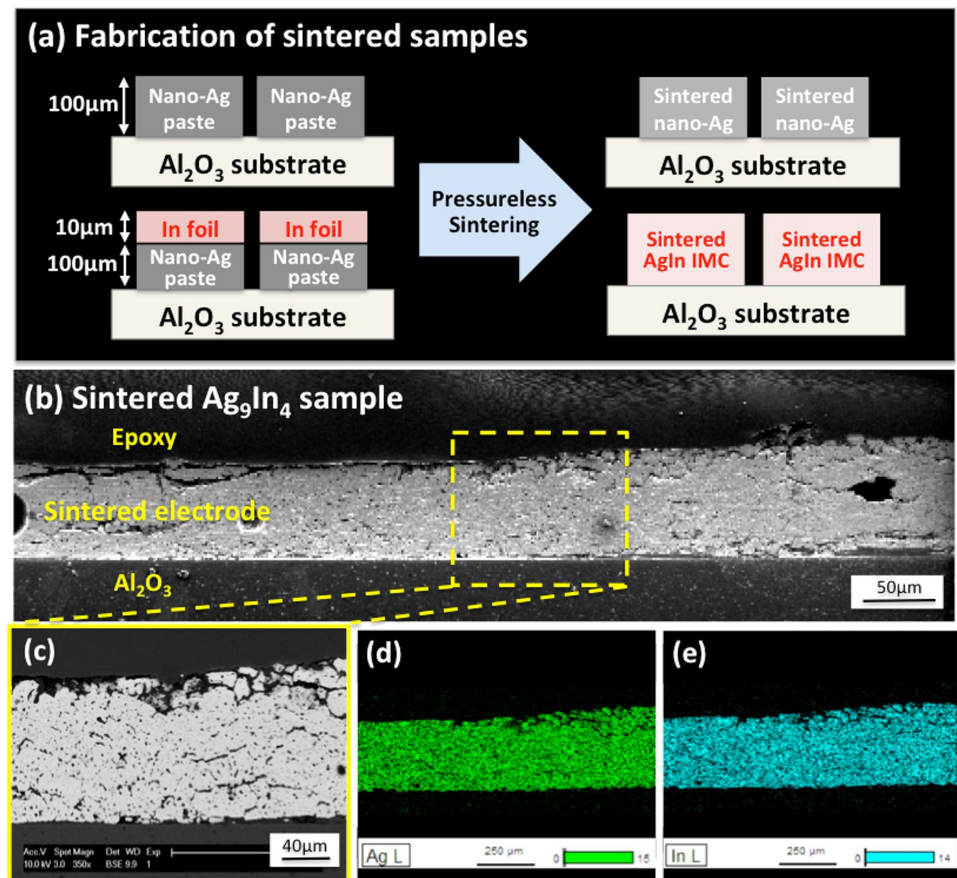

Fig. 2 **a** Fabrication process for the sintered samples and **b, c** the cross-sectional SEM images of a sintered Ag_9In_4 sample, and **d, e** its EDX elemental mappings

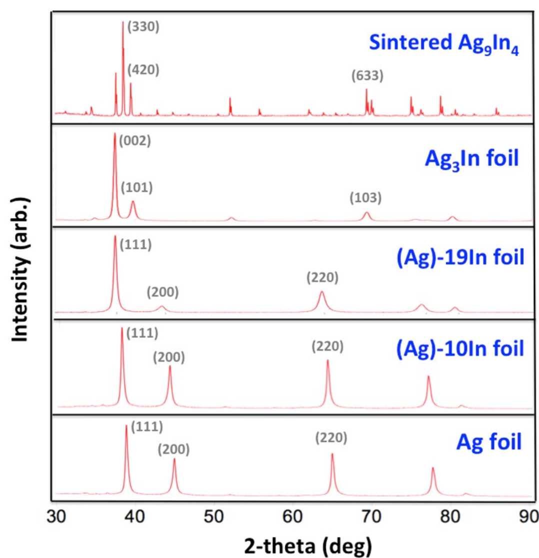

Fig. 3 XRD patterns of the electrode samples

solution samples, (Ag)-10In and (Ag)-19In foils. The SEM images and EDX results of the ten test locations on each sample are shown in Fig. 4. According to the results, the average compositions of (Ag)-10In foil and (Ag)-19In are Ag 90.4 at.% In 9.6 at.% with the error of ±0.88 at.%, and Ag 81.2 at.% In 18.8 at.% with the error of ±0.66 at.%, illustrating the compositions of the foils are in good uniformity.

2.3 Setup of the water drop test (WDT)

After identifying all the electrode samples, the test vehicle for the WDT was set up to analyze the ECM behavior of each electrode material. The schematic diagram and the actual sample setup of the configuration and specific dimensions of the test vehicle are shown in Fig. 5. The pair of the electrodes employed the same material and was separated by a gap of 2 mm, and was tightly fixed on the alumina substrate by fixing tape and fixture to make sure that no gap was between the electrodes and substrate. A pico-ammeter (Agilent B2902A Model) was utilized to measure the leakage current between the two electrodes during the WDT with the resolution of pA. A droplet of deionized water (resistivity 16.5 MΩ-cm) was placed on the gap between the two electrodes, and a voltage of 3 V was applied by attaching the probes of the pico-ammeter to the ends of two electrodes, as shown in Fig. 5a. WDTs were conducted at room temperature and the time to shortage was recorded.

Table 1 Summary of the crystallographic information of the electrode samples measured by XRD

Sample type	a (Å)	b (Å)	c (Å)	Alpha (°)	Beta (°)	Gamma (°)	Space group
Sintered Ag_9In_4	9.891	9.891	9.891	90	90	90	*P43m*
Ag_3In	2.970	2.970	4.799	90	90	120	*P63/mmc*
(Ag)-19In	4.154	4.154	4.154	90	90	90	*Fm3m*
(Ag)-10In	4.113	4.113	4.113	90	90	90	*Fm3m*
Ag	4.085	4.085	4.085	90	90	90	*Fm3m*

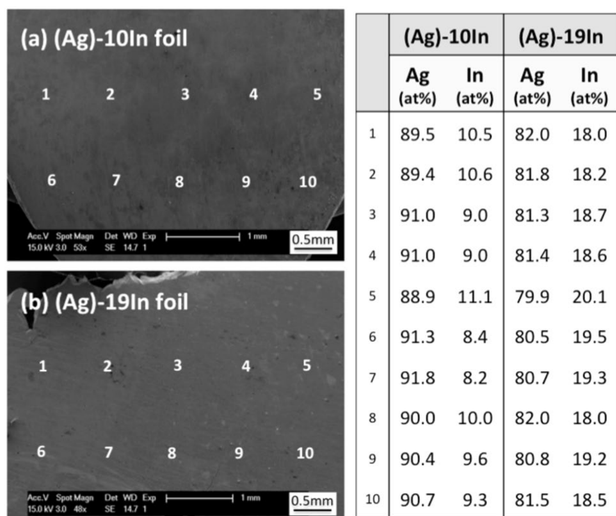

	(Ag)-10In		(Ag)-19In	
	Ag (at%)	In (at%)	Ag (at%)	In (at%)
1	89.5	10.5	82.0	18.0
2	89.4	10.6	81.8	18.2
3	91.0	9.0	81.3	18.7
4	91.0	9.0	81.4	18.6
5	88.9	11.1	79.9	20.1
6	91.3	8.4	80.5	19.5
7	91.8	8.2	80.7	19.3
8	90.0	10.0	82.0	18.0
9	90.4	9.6	80.8	19.2
10	90.7	9.3	81.5	18.5

Fig. 4 SEM images and EDX results of the ten test locations on **a** (Ag)-10In foil and **b** (Ag)-19In foil, respectively

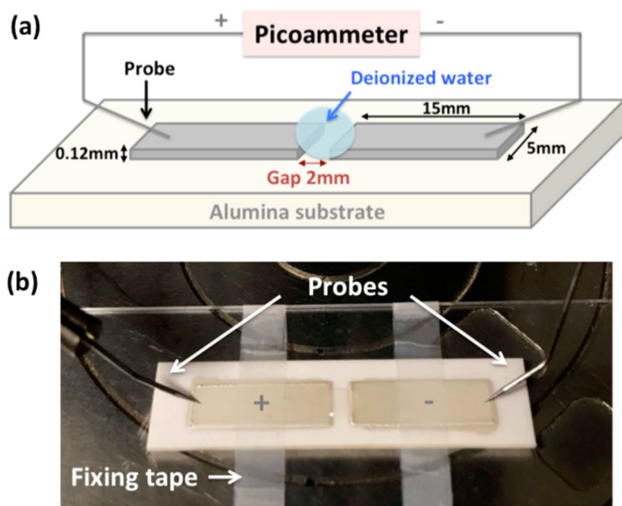

Fig. 5 Configuration and dimensions of the test vehicle for the WDT: **a** schematic diagram, **b** actual sample setup

The criterion for circuit shortage is when the leakage current reaches 10^{-4} A [1]. The morphologies of the dendrites between two electrodes and the surfaces of anode and cathode were observed and investigated by SEM and EDX. For

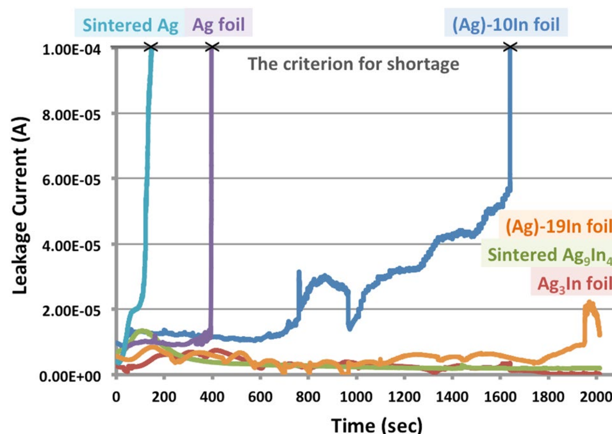

Fig. 6 The leakage current as a function of time for all tested electrodes during the WDT at 3 V

each kind of electrode sample, at least four WDTs have been carried out in order to obtain more objective understanding of their ECM behavior.

3 Results and discussion

3.1 Measurement of leakage current during the WDT

Figure 6 shows the leakage current measured by the picoammeter as a function of time for all tested electrodes during the WDT at 3 V. The duration before which a sample is shorted is defined as the "lifetime". A summary of the lifetime of all the electrode samples is presented in Table 2. All of the samples can be categorized into two material types: porous material or nonporous material for the distinction between sintered samples and foil samples. From Fig. 6, the leakage current of pure silver samples increased abruptly in a short time. The lifetime of Ag foil sample was two times longer than the sintered Ag sample. After adding 10 at.% indium into silver, the leakage current of (Ag)-10In foil sample gradually increased and did not reach the criterion for shortage until 1650 s. With a further increase of indium concentration in Ag–In alloys, (Ag)-19In foil, Ag_3In foil and sintered Ag_9In_4 samples did not form a short circuit even

Table 2 Summary of the lifetime of all the electrode samples during the WDT at 3 V and at room temperature

Lifetime during water drop test						
Electrode material	Porous materials		Nonporous materials			
	Sintered Ag	Sintered Ag_9In_4	Ag	Ag_3In	(Ag)-10In	(Ag)-19In
Lifetime (s)	146	> 2000	396	> 2000	1650	> 2000

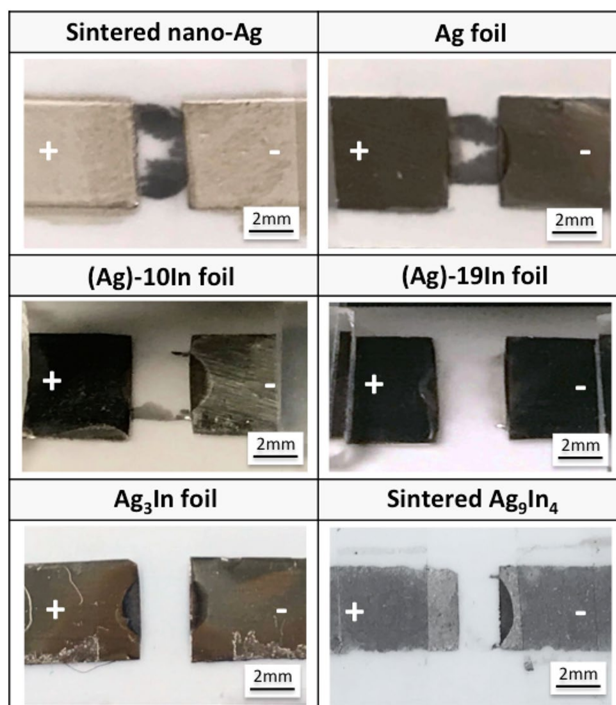

Fig. 7 The macroscopic images of the dendrite morphologies between two electrodes of each sample after the WDT

after 2000 s, and maintained a very low leakage current during the WDT.

Therefore, three conclusions can be drawn based on the above results. Firstly, porosity can degrade the resistance of samples to ECM due to the larger reaction surface areas and loose connection between silver particles, which has been reported elsewhere [4, 15]. Secondly, by alloying indium into silver material, the resistance of the samples to ECM significantly improves. Furthermore, the resistance of the samples to ECM can be further enhanced with higher indium concentration. Thirdly, both of the Ag–In intermetallic compounds, Ag_3In and sintered Ag_9In_4 samples, also have very high resistance to ECM at 3 V regardless of the porosity.

3.2 Observation of dendrite morphologies

Figure 7 shows the macroscopic images of the dendrite morphologies between two electrodes of each sample after the WDT. Silver dendrites in different materials grew in different morphologies. For pure silver samples, the dendrite morphology of sintered nano-Ag resembles the dendrites of Ag foil, appearing as two broad and spread-out dendrites growing along the edges of the water drop from the cathode (right side of the image) toward the anode (left side of the image). On the other hand, for (Ag)-10In foil samples, the two dendrites that grew out of the cathode along the edges of the water drop were narrow, and only one of them bridged the cathode and anode. As for (Ag)-19In and Ag_3In samples, no dendrite was observed between the electrodes after conducting the WDT for 2000 s, so the leakage current of both samples remained low during the tests. For the sintered Ag_9In_4 sample, although two small dendrites grew out of the cathode and also along the edges of the water drop, they stopped growing after conducting the WDT for 660 s and remained stable after 2000 s. Thus, the dendrites in the sintered Ag_9In_4 sample did not bridge between the two electrodes, resulting in a low leakage current throughout the test. It is worth noting that all of the dendrites seemed to grow along the edges of the water drop on the gap. This phenomenon results from the highest free energy at the ternary interface between liquid (water), gas (air) and solid (substrate), which is more favorable for the diffusion of silver ions and the nucleation of silver dendrites.

The microstructure of the dendrites was also analyzed by SEM. All the dendrites were basically composed of two types of dendrite structures in spite of the large difference in macroscopic morphologies of each sample. Figure 8 shows the SEM images of the two different dendrite types on (Ag)-10In sample, the thin dendrites and thick dendrites, and the zoom-in micrographs. The black background in each image represents the alumina substrate, and the grain morphology of alumina can clearly be seen in the enlarged micrographs in Fig. 8b–e. The lighter colors are silver dendrites that deposited on the alumina substrates, and they can be categorized into two types by the thickness (or the contrast shown in low magnification image in Fig. 8a): thin dendrites and thick dendrites, labeled as A and B in Fig. 8. In the thin dendrites section in Fig. 8d, a single layer of small silver dendrites was observed on the grains of alumina substrate, exposing the grain morphologies of the alumina substrate. On the other hand, many layers of silver dendrites had grown and covered the alumina substrate in the thick dendrites section, as shown in Fig. 8e, exposing a thick and flat silver layer without the appearance of alumina grains. The

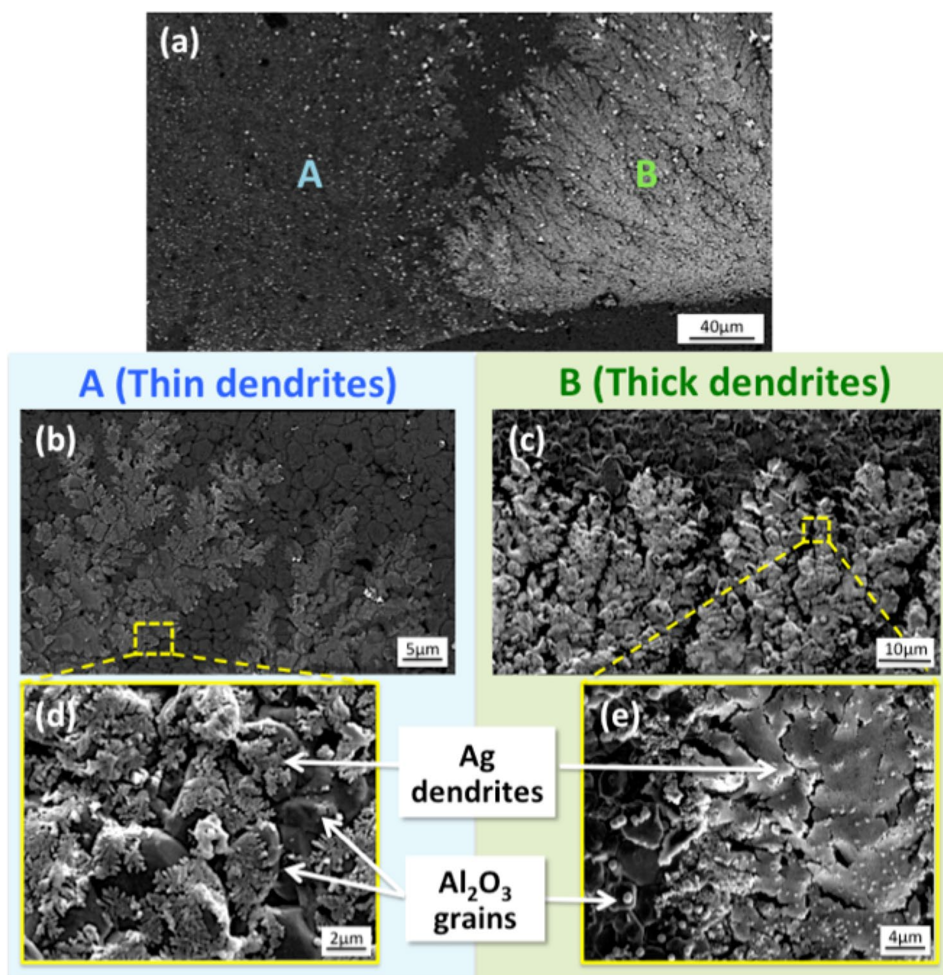

Fig. 8 SEM images of the two different dendrite types on (Ag)-10In sample, **a**–**c** thin and thick dendrites and **d, e** the zoom-in micrographs

formation of the two different types of silver dendrites has been reported in previous studies [6, 7], while the microstructures have not yet been analyzed in high magnification.

3.3 Analysis of the surface of anode electrode after the WDT

In order to investigate the anti-ECM mechanism in Ag–In alloys, the surfaces of the anode and cathode of each sample after the tests were analyzed. Only those regions that were covered by water during the WDT were examined, where the anodic and cathodic reactions, as well as ECM process, occurred the most.

Figure 9 shows the SEM images of the anode electrode surfaces after the WDT in the sintered Ag_9In_4 and (Ag)-19In samples, and the zoom-in micrograph from (Ag)-19In sample with EDX results. Indium oxide layers were found on the surfaces of both anodes. Figure 9c shows that some wrinkles, peeling and cracks were on the indium oxide layer. These were caused by the poor adhesion between the anode electrode and indium oxide layer, which might come from the impurities, defects and roughness on the surface of anode. From EDX results, the layer that covered the (Ag)-19In electrode (from point 1 to 4) was indium oxide (probably In_2O_3), and the locations where peeling occurred (point 5 and 6) exposed the surface of the original (Ag)-19In anode electrode. Furthermore, we could confirm again that the surface of the anode was covered with an indium oxide layer from the EDX elemental mappings of the anode surface in (Ag)-19In sample, as shown in Fig. 10. The strong signals of oxygen and indium could be acquired from this layer while the signal of silver was limited. As a comparison, silver and indium could be identified in the peeling area and the narrow cracks while the oxygen could hardly be found.

An indium oxide layer formed on the surface of the anodes in Ag–In alloys during the WDT, including (Ag)-10In, (Ag)-19In, Ag_3In and sintered Ag_9In_4 samples. The low ionic conductivity and low solubility properties of indium oxide enabled it to act as a passivation layer to the electrodes, thus inhibiting the dissolution of silver ions from the Ag–In alloys. In general, the ECM process involves three steps: the dissolution of metal ions, ion migration by electric field and diffusion, and dendrite formation and growth by electron transfer. Among the three, the dissolution step

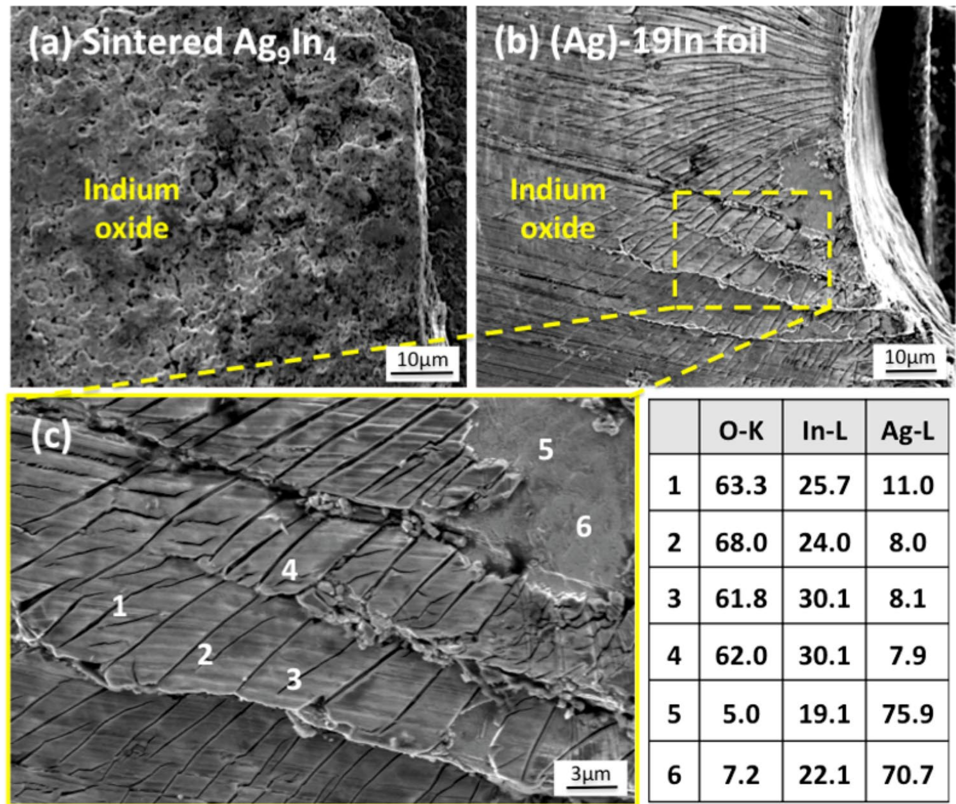

	O-K	In-L	Ag-L
1	63.3	25.7	11.0
2	68.0	24.0	8.0
3	61.8	30.1	8.1
4	62.0	30.1	7.9
5	5.0	19.1	75.9
6	7.2	22.1	70.7

Fig. 9 SEM images of the anode electrode surfaces after the WDT in **a** the sintered Ag_9In_4 sample, **b** (Ag)-19In sample, and **c** the zoom-in micrograph with EDX results

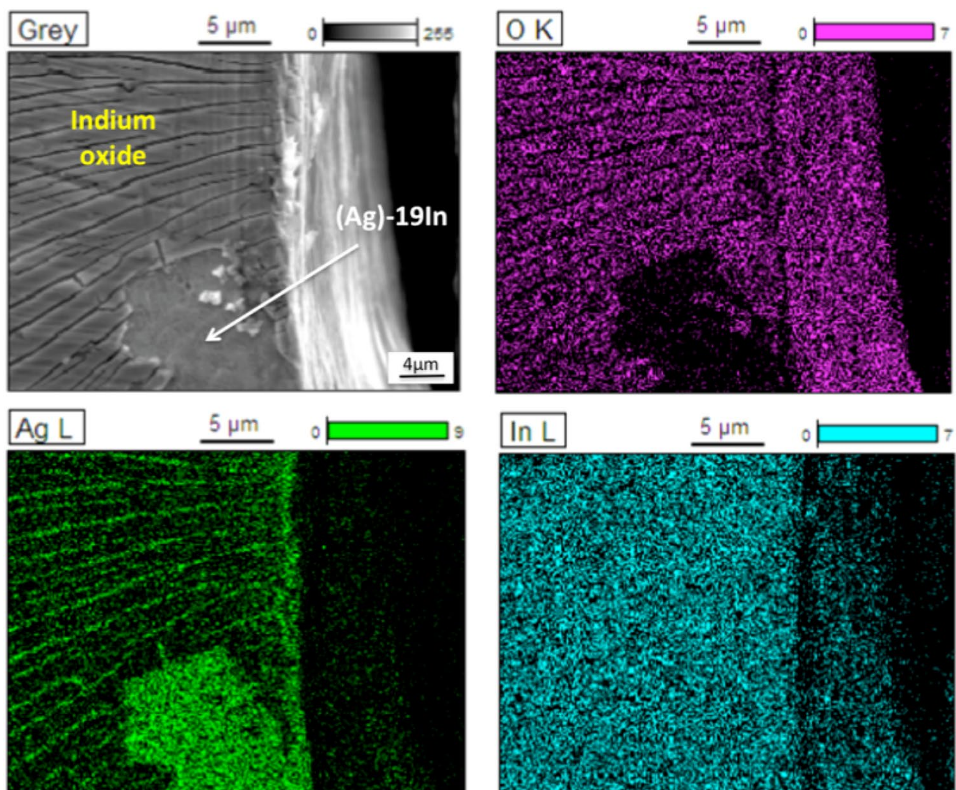

Fig. 10 EDX elemental mappings of the anode surface in the (Ag)-19In sample after the WDT

has been proved to be the rate-determining step in ECM process [2]. Therefore, the nature of the indium oxide layer on the anode would greatly slow down or completely inhibit the ECM process by blocking the dissolution path of silver ions, resulting in remarkably longer lifetime of Ag–In alloy samples.

Pure silver samples, including sintered nano-Ag and Ag foil samples, also formed silver oxide (either AgO or Ag_2O) on the surface of anodes in the beginning of the WDT. Nevertheless, silver oxides are relatively unstable and easy to break down under an electric field [6]. Thus, after a short incubation that was caused by the pseudo-passivation of silver oxide on the anode surface, silver oxide started to break down and massive dissolution of silver ions took place. Then, dendrites formed quickly and broadly across the gap to cause a sudden increase of the leakage current, resulting in short lifetime during the WDT.

3.4 Analysis of the surface of cathode electrode after the WDT

After the migration from the anode to cathode, silver ions receive electrons and deposit at the cathode electrode in the form of silver. The total amount and morphologies of reduced silver metal on the cathode depends on the material of the electrode sample. Figure 11 shows the SEM images of the cathode electrode surfaces in Ag foil and (Ag)-10In samples after the WDT. Both of the cathodes were covered by numerous silver precipitates, illustrating the massive ECM process of silver ions occurred during the WDT and left a lot of reduced silver depositions on the cathodes. In Fig. 11a, bunches of needle-like (or dendrite-like) silver precipitates with the dimension of several microns grew on the cathode of the pure silver sample. The amount of silver precipitates on the cathode decreased as the distance increased from the gap, which means a longer distance that silver ions had to travel from the anode to the place where they were reduced. As for the cathode in (Ag)-10In sample that is shown in Fig. 11b, small and relatively round silver particles with the dimension < 100 nm were deposited on the surface, and the amount also decreased as the distance increased from the gap. As for the (Ag)-19In, Ag_3In and sintered Ag_9In_4 samples in which ECM process barely took place, only a few silver particles could be found on the surface of each cathode.

In conclusion, the difference on surface morphology of the cathode in each sample results from the amount of silver that participated in the ECM process during the WDT. As more silver ions dissolved from the anode, more silver metal was deposited on the surface of cathode, which led to more silver dendrites that formed and grew between the electrodes, as shown in Fig. 7.

3.5 Anti-electrochemical migration mechanism in Ag–In alloys

The mechanism of silver ECM in thick pure silver films has been proposed [16]. From the WDT results in our studies, we found that the silver migration behavior was significantly suppressed in the presence of indium, and as the concentration of indium in the Ag–In solid solution increased, the anti-ECM property was more obvious. Both Ag_9In_4 and Ag_3In also exhibited excellent anti-ECM properties. The anti-ECM mechanism of Ag–In alloys needs to be understood.

According to the analysis of the reaction products on the surfaces of electrodes and the observation of ECM behavior, the anti-ECM mechanism can be ascribed to the passivation of the indium oxide (In_2O_3) layer, which is formed on the surface of anodes by anodic polarization during the WDT. Considering the standard reduction potential for silver and indium metals [18]:

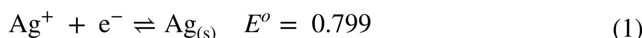

$$Ag^+ + e^- \rightleftharpoons Ag_{(s)} \quad E^o = 0.799 \tag{1}$$

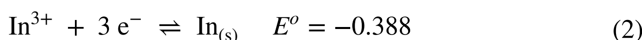

$$In^{3+} + 3\,e^- \rightleftharpoons In_{(s)} \quad E^o = -0.388 \tag{2}$$

A reduction reaction for indium ion (In^{3+}) is harder to take place than for silver ion (Ag^+), which means that

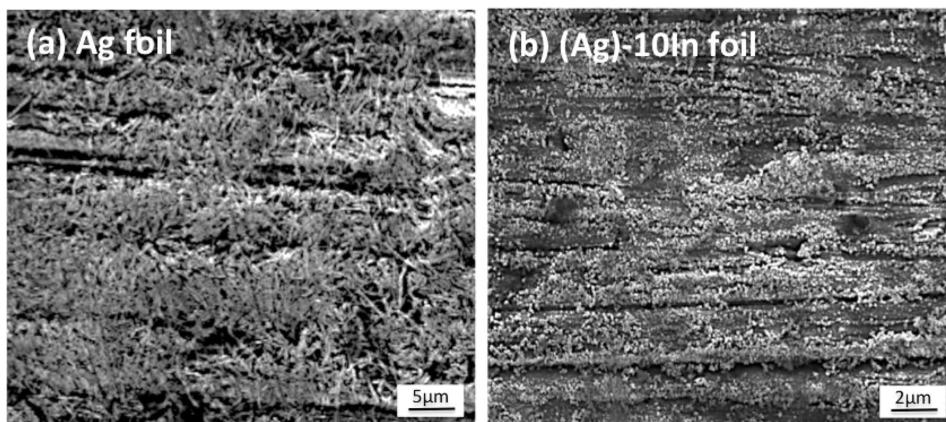

Fig. 11 SEM images of the cathode electrode surfaces in **a** Ag foil sample and **b** (Ag)-10In sample after the WDT

indium metal can oxidize at relatively lower potential than silver metal, so it is much easier for indium metal to oxidize (anodic reaction) and become indium ions (In^{3+}) in the Ag–In alloy samples. Then, In^{3+} ions combine with OH^- ions, which is dissociated from water:

$$H_2O \rightleftharpoons H^+ + OH^- \quad (3)$$

to form $In(OH)_3$. Due to the massive oxidation reaction of indium from Eq. (2), concentrated In^{3+} ions instead of Ag^+ ions accumulate around the anode and form numerous $In(OH)_3$. However, $In(OH)_3$ is unstable so it might decompose as described in Eq. (4) below,

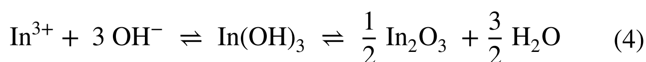

$$In^{3+} + 3\,OH^- \rightleftharpoons In(OH)_3 \rightleftharpoons \frac{1}{2}\,In_2O_3 + \frac{3}{2}\,H_2O \quad (4)$$

Thus, the overall anodic reaction is represented as,

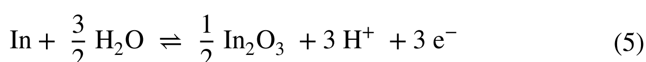

$$In + \frac{3}{2}\,H_2O \rightleftharpoons \frac{1}{2}\,In_2O_3 + 3\,H^+ + 3\,e^- \quad (5)$$

Indium metal rapidly oxidized in deionized water during the WDT, and formed In_2O_3 on the surface of the anode in Ag–In alloy samples.

Figure 12 shows the schematic diagrams of the anti-ECM mechanism in the Ag–In alloy samples. For pure silver samples, silver ions could basically dissolute from anywhere on the surface of the anode electrode, no matter if they are from pure silver or silver oxide [6]. The massive dissolution of silver ions from the anode participates in the ECM process to lead to broadly distributed and rapidly growing silver dendrites between the electrodes, as shown in Fig. 7. As for Ag–In solid solution samples, the indium oxide layer forms instantly on the anode prior to silver dissolution or silver oxide formation, thus inhibiting the ECM process by blocking silver atoms on the surface from exposing themselves to the water. With 10 at.% of indium, indium oxide layer can form on the surface of the anode to considerably reduce the amount of silver dissolution by passivating most of the reaction area, resulting in a significantly prolonged lifetime (roughly from 400 to 1650 s) as well as narrowly distributed silver dendrites that shown in Fig. 7. With higher indium concentration, more indium atoms surround the surface and turn into a continuous indium oxide layer on the anode during the WDT. Then, the indium oxide layer provides a complete anodic passivation to the sample so that the ECM process is inhibited.

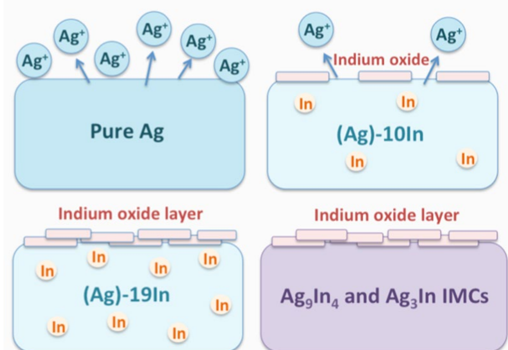

Fig. 12 Schematic diagrams illustrating the anti-ECM mechanism in Ag–In alloy samples

As for Ag–In intermetallic compounds, a continuous and dense indium oxide layer also forms on the anode during the WDT, which results in the anti-ECM property to the sample. Nevertheless, two narrow dendrites can still be observed in the sintered Ag_9In_4 sample, as shown in Fig. 7. This phenomenon might come from two possible reasons. Firstly, small amount of sintered nano-Ag can remain in the sintered Ag_9In_4 electrode due to nonuniform compositional distribution in sintered electrodes. Secondly, small amount of silver may dissolute before the indium oxide fully covers the anode surface considering that the sintered electrode has larger surface area. Only small dendrites are formed before the inhibition of the ECM process and the growth of silver dendrites. In conclusion, the resistance of the samples to ECM is significantly improved by alloying indium into silver material, including (Ag)-10In, (Ag)-19In, Ag_3In, and Ag_9In_4.

3.6 The influence of the surface quality on anti-ECM mechanism

The surface quality of the electrodes is also an important factor in the WDT. Figure 13 shows the SEM images of pitting corrosion and peeling that occurred occasionally on the anode surfaces of the Ag_3In and (Ag)-19In samples. Impurities, voids and inclusions that were embedded in the foil samples during the foil fabrication process such as ingot casting and rolling process would give rise to the pitting corrosion on the anode during the WDT. Pitting corrosion broke down the passivation of the indium oxide layer on the anode, as shown in Fig. 13a, and created a path for silver dissolution. Moreover, surface roughness of the foil samples after rolling process and polishing as well as the intrinsically poor adhesion between the Ag–In alloys and indium oxide layer would lead to peeling and the formation of cracks in the indium oxide layer, and cause the failure of anti-ECM mechanism. Therefore, some early shortage failures might occur in the Ag–In alloy samples during the WDT.

However, of all Ag–In alloys, the materials themselves still possess inherent and excellent anti-ECM property due to the nature of indium oxide passivation under humidity and electric field. Therefore, to achieve high ECM resistance, surface quality on the electrode is essential for the alloy to realize its anti-ECM property. The quality control of the electrode including purity, low defects, and surface

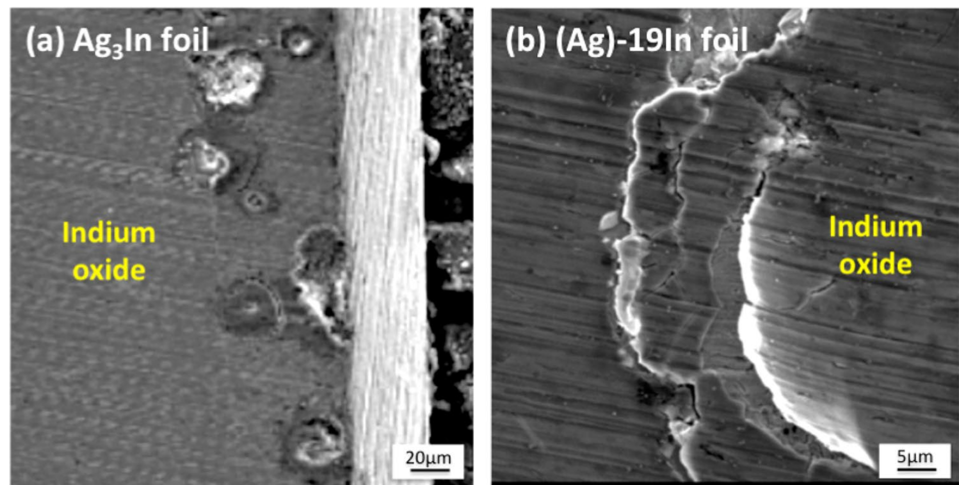

Fig. 13 SEM images of pitting corrosion and peeling occasionally occurring on the anode surfaces of **a** a Ag_3In sample and **b** a (Ag)-19In sample, respectively

smoothness, is relatively easy in production environment in industries. Besides, it is more cost effective to use indium instead of palladium as the alloying element, illustrating the high possibility of the Ag–In alloy being a feasible replacement for the commonly used Ag–Pd alloy.

4 Conclusion

The ECM resistance of silver was significantly improved by alloying indium into silver material. The lifetime became four times longer after alloying 10 at.% of indium to form the Ag–In solid solution. As the indium concentration reaches 19 at.%, the ECM was completely suppressed. The microscopic morphology of the dendrites in each sample was similar. However, the macroscopic morphology of the dendrites in pure silver samples was much broader than the dendrites in (Ag)-10In sample because more silver had dissolved from the anode. In addition, no bridging dendrites were formed in (Ag)-19In, Ag_3In, and sintered Ag_9In_4 samples due to the complete passivation of the anode by the indium oxide layer.

The anti-ECM mechanism of the Ag–In alloy samples works by forming an indium oxide layer on the surface of the anode as an anodic passivation to block silver dissolution from anode during the WDT, consequently inhibiting the ECM process. To realize the anti-ECM potential of these Ag–In alloys, the surface quality of the electrodes is critical. Impurities, defects, inclusions, and roughness can degrade the quality of passivation layer, thus reducing its anti-ECM performance. In conclusion, Ag–In alloys, including (Ag)-10In, (Ag)-19In, Ag_3In, and Ag_9In_4, exhibit excellent resistance to ECM in deionized water and at 3 V. They are valuable as promising candidates for conductor, metallization, and interconnection materials in fine pitch and high power electronic devices.

Acknowledgements The financial supports of Ministry of Education of Taiwan through grant 107L9006 and Ministry of Science and Technology of Taiwan through grants 107-3017-F-002-001 and 104-2221-E-002-040-MY3 are acknowledged. The Advanced Research Center of Green Materials Science and Technology is supported by the Featured Areas Research Center Program within the framework of the Higher Education Sprout Project of Taiwan. The authors would like to thank Prof. Peter Burke of the Department of Electrical Engineering and Computer Science in University of California, Irvine for providing the pico-ammeter equipment, and Industrial Technology Research Institute of Taiwan for providing the nano-silver paste.

References

1. B. Medgyes, B. Illes, G. Harsanyi, Electrochemical migration behaviour of Cu, Sn, Ag, and Sn63/Pb37. J. Mater. Sci.: Mater. Electron. **23**, 551–556 (2012)
2. M.S. Jung, S.B. Lee, H.Y. Lee, C.S. Ryu, Y.G. Ko, H.W. Park, Y.C. Joo, Improvement of electrochemical migration resistance by Cu/Sn intermetallic compound barrier on Cu in printed circuit board. IEEE Trans. Dev. Mater. Reliab. **14**(1), 382 (2014)
3. D.Q. Yu, W. Jillek, E. Schmiitt, Electrochemical migration of Sn–Pn and lead free solder alloys under distilled water. J. Mater. Sci.: Mater. Electron. **27**, 219–227 (2006)
4. J.W. Yoon, B.I. Noh, S.B. Jung, Electrical properties and electrochemical migration characteristics of directly printed Ag patterns with various sintering conditions. Microelectron. Reliab. **54**, 410–416 (2014)
5. T. Takemoto, R.M. Latanision, T.W. Eagar, A. Matsunawa, Electrochemical migration tests of solder alloys in pure water. Corros. Sci. **39**, 1415–1430 (1997)
6. J.C. Lin, J.Y. Chan, On the resistance of silver migration in Ag-Pd conductive thick films under humid environment and applied d.c. field. Mater. Chem. Phys. **43**, 256–265 (1995)
7. J.C. Lin, J.Y. Chuang, Resistance to silver electrolytic migration for thick-film conductors prepared from mixed and alloyed powders of Ag-15Pd and Ag-30Pd. J. Electrochem. Soc. **144**(5), 1652–1659 (1997)
8. C.A. Yang, C.R. Kao, H. Nishikawa, Development of die attachment technology for power IC module by introducing indium into sintered nano-silver joint. In *The IEEE 67th Electronic Components and Technology Conference (ECTC)*, San Diego, 2017

9. C.A. Yang, C.R. Kao, H. Nishikawa, C.C. Lee, High reliability sintered silver-indium bonding with anti-oxidation property for high temperature applications. In *The IEEE 68th Electronic Components and Technology Conference (ECTC)*, San Diego, 2018
10. C.A. Yang, S. Yang, X. Liu, H. Nishikawa, C.R. Kao, Enhancement of nano-silver chip attachment by using transient liquid phase reaction with indium. J. Alloys Compd. (2018). https://doi.org/10.1016/j.jallcom.2018.05.254
11. Y.Y. Wu, D. Nwoke, F.D. Barlow, C.C. Lee, Thermal cycling reliability study of Ag-In joints between Si chips and Cu substrates made by fluxless processes. IEEE Trans. Compon. Packag. Manuf. Technol. **4**(9), 1420–1426 (2014)
12. Y. Huo, J. Wu, C.C. Lee, Study of anti-tarnishing mechanism in Ag–In binary system by using semi-quantum-mechanical approach. J. Electrochem. Soc. **164**(7), C418–C427 (2017)
13. B.I. Noh, S.B. Jung, Characteristics of environmental factor for electrochemical migration on printed circuit board. J. Mater. Sci.: Mater. Electron. **19**, 952–956 (2008)
14. B.I. Noh, J.B. Lee, S.B. Jung, Effect of surface finish material on printed circuit board for electrochemical migration. Microelectron. Reliab. **48**, 652–656 (2008)
15. G.Q. Lu, W. Yang, Y.H. Mei, X. Li, G. Chen, X. Chen, Mechanism of migration of sintered nano-silver at high temperatures in dry air for electronic packaging. IEEE Trans. Dev. Mater. Reliab. **14**(1), 311–317 (2014)
16. T. Kawanobe, K. Otsuka, Metal migration in electronic components. In *IEEE Transactions on Components, Hybrids, and M. Technology, CHI-781*, pp. 220–228 (1982)
17. Z. Bahari, J. Rivet, B. Legendre, J. Dugué, Study of the Ag-In-Te ternary system. II. Description of the quadrilateral Ag-Ag2Te-In2Te3-In. J. Alloys Compd. **289**, 99–115 (1999)
18. D.C. Harris, *Quantitative Chemical Analysis*, 7th edn. (W.H. Freeman, Company, New York, 2006), (**APPENDIX H**)